Self-assembly of biological networks via adaptive patterning revealed by avian intradermal muscle network formation

Xiao-shan Wu[a,b,c,1], Chao-yuan Yeh[a,d,1], Hans I-Chen Harn[a,e], Ting-Xing Jiang[a], Ping Wu[a], Randall B. Widelitz[a], Ruth E. Baker[f], and Cheng-Ming Chuong[a,d,e,2]

[a]Department of Pathology, University of Southern California, Los Angeles, CA 90033; [b]Department of Oral and Maxillofacial Surgery, Xiangya Hospital, Central South University, 410008 Changsha, China; [c]Molecular Laboratory for Gene Therapy and Tooth Regeneration, Beijing Key Laboratory of Tooth Regeneration and Function Reconstruction, Capital Medical University School of Stomatology, 100050 Beijing, China; [d]Integrative Stem Cell Center, China Medical University, 40402 Taichung, Taiwan; [e]International Research Center of Wound Repair and Regeneration, National Cheng Kung University, 701 Tainan, Taiwan; and [f]Mathematical Institute, University of Oxford, OX2 6GG Oxford, United Kingdom

Edited by Brigid L. M. Hogan, Duke University Medical Center, Durham, NC, and approved April 9, 2019 (received for review October 29, 2018)

Networked structures integrate numerous elements into one functional unit, while providing a balance between efficiency, robustness, and flexibility. Understanding how biological networks self-assemble will provide insights into how these features arise. Here, we demonstrate how nature forms exquisite muscle networks that can repair, regenerate, and adapt to external perturbations using the feather muscle network in chicken embryos as a paradigm. The self-assembled muscle networks arise through the implementation of a few simple rules. Muscle fibers extend outward from feather buds in every direction, but only those muscle fibers able to connect to neighboring buds are eventually stabilized. After forming such a nearest-neighbor configuration, the network can be reconfigured, adapting to perturbed bud arrangement or mechanical cues. Our computational model provides a bioinspired algorithm for network self-assembly, with intrinsic or extrinsic cues necessary and sufficient to guide the formation of these regenerative networks. These robust principles may serve as a useful guide for assembling adaptive networks in other contexts.

feather | skin appendage | morphogenesis | regeneration | network assembly

A population of independently positioned elements can interconnect to form networks with different configurations dependent upon inherent and environmental factors (1–3). Different network configurations may possess different properties, such as higher stability or higher plasticity to self-realign after damage. If the number or position of elements is altered through damage, the network could then be reconfigured in response to the contextual environment. The properties of this new network configuration would be expected to be altered from those of the original configuration. Research on network formation has garnered a lot of interest in the past decade, facilitated by converging studies across different fields, such as sociology, computer science, animal behavior, mathematics, and biology (2, 4). In many cases, special network configurations are formed via a top-down human design. We are motivated to learn the factors that guide the formation of natural biological networks that have been distilled by evolution and can self-assemble, self-repair, and adapt to changing environments. We hope to learn some of these bioinspired principles, which may help us build better networks.

To accommodate flight and coordinate the thousands of feathers on the body surface, birds have evolved appendage muscle systems that move wings and legs, as well as an integumentary muscle system consisting of a layer of intradermal smooth muscle and a layer of striated subcutaneous muscle (5). The intradermal muscle layer is composed of a network interconnecting erector and depressor smooth muscle fibers, forming a flexible 2D grid network that integrates many feather follicles into one functional unit. The subcutaneous striated muscle layer works with this musculoelastic layer to form an integrative integumentary muscle system that can respond to mechanical strain over the body surface, controlling the body contours and assisting in flight (5). Understanding how this complex mechanoresponsive muscle system is formed may help us identify fundamental principles that can be used in human designed network formation. Here, we use the developing chicken skin to study the assembly of this functional network.

The developing chicken skin is an established multiscale model for pattern formation (6). Periodic patterning allows a field to become a composition of multiple elements. Since each element has its own stem cells that can undergo cyclical renewal, each element can regenerate into distinct forms. The combination of diverse forms in these multiple elements gives rise to complex pattern formation (7). We propose that the integument pattern is built at multiple levels. At the first level, de novo periodic patterning involving Turing principles guides the emergence of periodically arranged feather primordia from the nonpatterned morphogenetic field (8). At the second level, adaptive pattern formation, the next level of cells (e.g., muscle, blood vessels, nerve fibers) is assembled into networks using the periodically arranged feather primordia as reference points. In mammals, hair arrector pili muscles connect each follicle to the basal layer of skin epidermis (9), but there are no physical links among different hair follicles. In contrast, in birds,

Significance

Humans have the most elaborate facial expressions, controlled by muscle networks anchored at distinct sites within the facial skin. Here, we reveal how muscle networks assemble robustly, adapting to external perturbations and insults, using avian intradermal muscle networks as a model. The muscle network is established with simple, local rules. Muscle fibers extend from feather buds in every direction, and connect to nearest neighbor buds. The network can be reconfigured, adapting to perturbed bud arrangement or mechanical cues. Our computational model validates the local rules, providing a potential mechanism for forming adaptive networks that could be useful in understanding other biological networks or designing nonbiological networks.

Author contributions: C.-M.C. conceived the concept; C.-M.C., X.-s.W., and C.-y.Y. designed the experiments; X.-s.W., C.-y.Y., H.I.-C.H., T.-X.J., and R.E.B. performed research; X.-s.W. and C.-y.Y. analyzed data; and X.-s.W., P.W., R.B.W., R.E.B., and C.-M.C. wrote the paper.

The authors declare no conflict of interest.

This article is a PNAS Direct Submission.

[1]X.-s.W. and C.-y.Y. contributed equally to this work.

[2]To whom correspondence should be addressed. Email: cmchuong@usc.edu.

This article contains supporting information online at www.pnas.org/lookup/suppl/doi:10.1073/pnas.1818506116/-/DCSupplemental.

Published online May 9, 2019.

feather muscles interconnect all follicles in the same tract into an array. Both depressor and erector muscles interconnect two adjacent buds forming a "criss-crossing" structure that forms the 2D muscle network in the thin dermis (10). The muscle network configurations differ in different body regions, displaying specific regional patterning among dorsal-pelvic, ventral, femoral, and apteric tracts (10). Since thousands of muscle fiber bundles are assembled within one area of the skin, it seems unlikely that each muscle bundle has been given a unique identity and the network is assembled from the top down. Instead, we hypothesize that the bird dermal muscle network self-assembles using only local "bottom-up" rules, making it robust to perturbations and efficient to control and modulate. Thus, we set out to identify these basic rules in the intradermal smooth muscle network, with the hope that these principles can be useful toward human engineered network formation.

In this study, using the chicken feather muscle network as a model, we reveal an adaptive patterning process and unveil its regulatory mechanisms. First, we characterize the developmental stages of feather muscle patterning and identify the spatial and temporal principles underlying 2D network assembly. We show that the muscle network topology is pleomorphic across different skin regions, reflecting both modularity and flexibility. In addition, these networks can adapt to changing feather topologies after recombination, reconstitution, and microsurgery experiments. Mechanical force is found to be one of the guiding cues in muscle fiber migration and is shown to regulate muscle patterning.

Our multidisciplinary approach demonstrates that the formation of a network pattern, using the feather dermal muscle network paradigm, can occur through a robust and adaptive self-organizing process that does not require a specific blueprint. Using existing feather buds as reference points, the initially randomly distributed muscle fibers are gradually aligned and organized into one network. The connection represents a stable, but not permanent, state, with dynamic equilibrium. Thus, the muscle network can adapt to changing environments; it can reconfigure if a node is missing or the orientation of tension within the skin is altered.

Results

Intradermal Smooth Muscle Networks in Chicken Skin Display Region-Specific Configurations. Chicken feather buds form a highly ordered array that becomes a functional unit through the attachment of interconnecting smooth muscle bundles. The dorsal body is covered by the dorsal-pelvic skin tract, while the thigh is covered by the femoral tract. The area between them in lateral regions of the body forms sparse feathering and is called the apteric tract (10) (Fig. 1*A* and *SI Appendix*, Fig. S1). Connections between two adjacent buds actually contain both erector and depressor muscles, which function to raise or lower feathers. Depending on the muscle insertion sites on the feather follicle, the erector and depressor muscles form intercrossing 3D structures (10). Starting around embryonic day 10 (E10), feather buds start to invaginate and remodel into feather follicles. Tenascin C-positive regions (orange) are found surrounding the base of forming feather follicles and serve as anchoring sites of distinct muscle types (Fig. 1 *B* and *B′*).

Since the dorsal-pelvic tract has higher feather density than the femoral tract which, in turn, displays a higher density than the apteric tract (*SI Appendix*, Fig. S2*A*), we hypothesize that feather follicle density might affect the spatial configuration of the muscle network. Indeed, we find that feather density does affect the spatial configuration of the muscle network. In the dorsal-pelvic tract, where feather buds are hexagonally arranged, each bud has connections to its six neighbors (Fig. 1 *C* and *G*). In the femoral tract, where feather buds are tetragonally arranged, each bud is connected by muscles to its four nearest neighbors (Fig. 1 *D* and *H*). This regular patterning is not apparent in the apteric tract, where the feather bud density is only about one-third the density of the dorsal-pelvic tract and feather buds are randomly distributed. Rather thin and separate muscle bundles are predominantly organized along the medial-lateral axis and can connect more distant feather buds (Fig. 1*E*). The lengths of the muscle fibers in the apteric tract are significantly longer than in the other two tracts (*SI Appendix*, Fig. S2*B*).

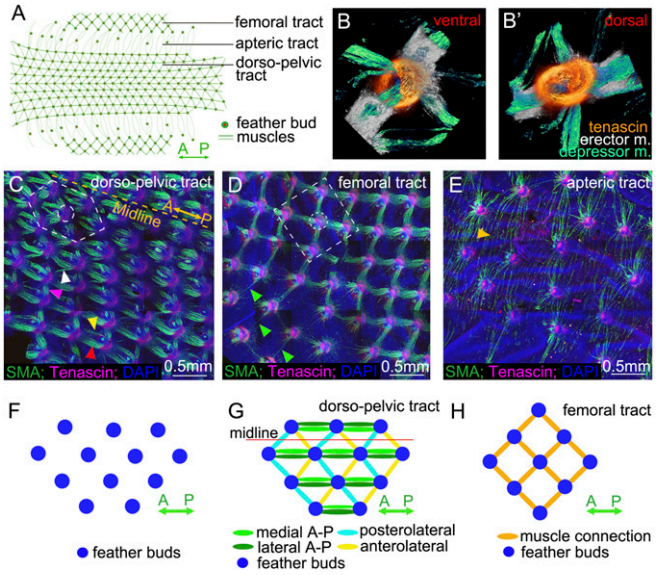

Fig. 1. Intradermal muscle network is present in the skin of birds. (*A*) Schematic diagram of the dorsal-pelvic, femoral, and apteric tracts of chicken skin showing region-specific configurations. (*B* and *B′*) Ventral and dorsal views of the 2D feather muscles beneath a bud shows the criss-cross depressor and erector muscles (m.) attached to the tenascin domains. (*C*–*E*) Images of feather muscle patterns in dorsal-pelvic, femoral, and apteric tracts at E12, stained with α-SMA (green), tenascin C (red), and DAPI (blue). Dotted white lines show the hexagonal (dorsal-pelvic tract) and tetragonal (femoral tract) feather patterns. Width of *B* is 500 μm. (*C*) Hexagonal configuration in the dorsal-pelvic tract. The dotted yellow line represents the midline (A-P). Two rows of muscle bundles connect along the A-P axis (yellow and red arrowheads). There are two kinds of lateral connections (anterolateral, white arrowhead; posterolateral, purple arrowhead) ($n = 20$). (*D*) Tetragonal configuration in the femoral tract; single muscle fibers connect with tenascin C domains on feather buds before the muscle bundle develops (green arrowheads) ($n = 20$). (*E*) Long and thin muscle fibers connect two distant feather buds in the apteric tract (golden arrowhead) ($n = 20$). (*F*) Schematic drawing of the feather bud array with multiple options for potential connection. (*G*) Schematic drawing of the hexagonal configuration in the dorsal-pelvic tract. (*H*) Schematic drawing of the tetragonal configuration in the femoral tract.

In the dorsal-pelvic tract, three orientations of muscle bundles can be identified: posterolateral, anterolateral, and longitudinal [anterior-posterior (A-P) axis] (Fig. 1 *C* and *G*). The thickness of the muscle bundles differs between these different orientations. The longitudinal connection, containing two rows of muscle bundles, is the thickest. The posterolateral connection is thinner, and the anterolateral connection is the thinnest (*SI Appendix*, Fig. S2*C*).

Feather bud arrays form at E7 when muscle connections have not yet been established (Fig. 1*F*). There are many possible ways to connect a population of feather buds, either with a hexagonal arrangement of muscle fibers, as in the dorsal-pelvic tract (Fig. 1*G*), or with a tetragonal arrangement, as in the femoral tract (Fig. 1*H*). The difference could be due to regional different environmental properties, such as bud density or local skin tension, but remains to be studied.

Stepwise Assembly of the Muscle Network. We next explore how the network is assembled using the dorsal-pelvic tract as a model. Here, the development of the muscle network begins at E8 and is almost complete by E12. Tenascin C, a protein highly enriched in

tendons, is expressed in four distinct topological domains surrounding each bud. We sequentially mark these tenascin C topological domains 1–4 according to the order in which they are established. The formation of tenascin C domains always precedes muscle fiber anchoring. The depressor muscle is anchored between tenascin C domains 2 and 3, while the erector muscle is anchored between tenascin C domains 1 and 4 (Fig. 2 *A*–*D*).

We divide the developmental process into seven stages (Fig. 2 *A*–*C*). Tenascin C is first expressed in the anterior and posterior upper dermis (domains 1 and 2; stage 1). Later, smooth muscle actin (SMA) expression appears in the anterior facet of tenascin C domain 2 (stage 2). Tenascin C domain 3 appears posterior to domain 2 (stage 3), and the depressor muscle connection forms between domain 2 of one bud and domain 3 of the neighboring bud (stage 4). Tenascin C domain 4 develops beneath domains 2 and 3 (stage 5), and the erector muscle connection forms between domain 4 of one bud and domain 1 of its neighboring bud (stage 6). The 2D network is mature at stage 7 (Fig. 2*A*). This process is also illustrated in a schematic drawing (Fig. 2 *B*–*D*).

The positive staining of SMA shows feather muscle is smooth muscle. Also, feather muscle is positive for myosin staining (*SI Appendix*, Fig. S3*A*). Feather muscle is localized in the dermis. It is known that the origin of dorsal dermis is from dermomyotome (11, 12). The staining of Pax3 and Myod showed the possible migration of the precursor cells from the myotome (12) (*SI Appendix*, Fig. S3 *B* and *C*). However, we will focus here on the assembly of the smooth muscle network.

Smooth Muscle Connection and Anchoring Formation. Our aim was to understand how muscle precursor cells find their anchoring sites. In the dorsal-pelvic tract, we find that muscle fibers migrate out of individual feather buds at E9, at a wide range of angles with respect to the bud of origin (Fig. 3*A*). Within 1 d, refined depressor muscle bundle connections are established between buds, with few unconnected muscle fibers remaining (Fig. 3*B*). Muscle precursors initially migrate out from the origin bud radially and cover the great majority of interbud space (Fig. 3 *C*–*E*). These muscle cells become anchored and stabilized when touching the tenascin C-positive regions of neighboring buds (Fig. 3 *F*–*H*). When they are anchored at E10, the muscle cells become elongated and form bundles (Fig. 3 *I* and *J*).

To study whether all muscle cells eventually stabilize or not, we carried out a TUNEL assay on the developing skin. There were very few TUNEL-positive cells in the 0.08-mm^2 dermis at E9, while there were, at most, 10 cells in the 0.08-mm^2 dermis at E10 (*SI Appendix*, Fig. S4). Therefore, while we cannot completely rule out the presence of an apoptotic event(s), it does not seem to be a major event. More study is necessary in the future.

We have found the tenascin C-positive regions surround the base of feather buds and serve as sites of muscle connections. Cell surface receptors for the tenascins include members of the

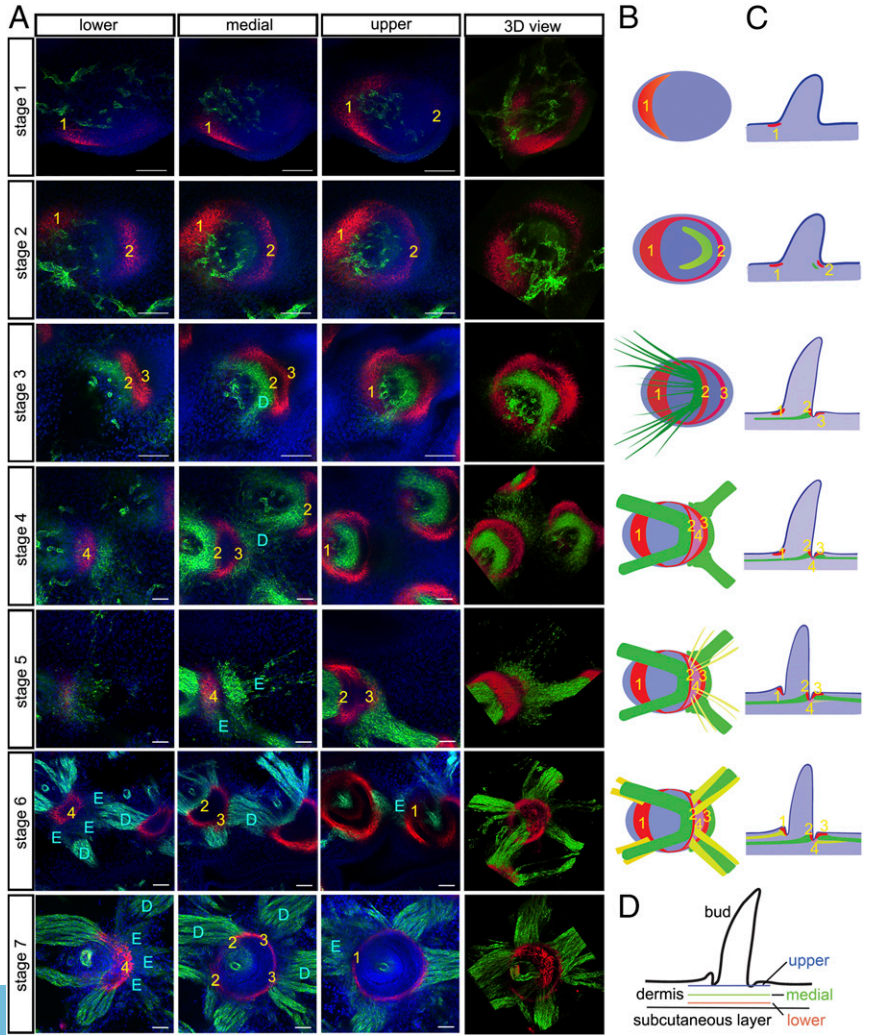

Fig. 2. Stepwise assembly of the muscle network. (*A*) Images of a single muscle network node at different developmental stages (1–7). Whole-mount developing chicken skin is immunostained with SMA (green), tenascin C (red), and DAPI (blue). Four tenascin domains (indicated by yellow numbers) and depressor (D) and erector (E) muscles can be identified. At stage 1, the anterior tenascin domain 1 (T1) appears, followed by the posterior tenascin domain (T2). At stage 2, the posterior end of the depressor muscle develops in the center of a bud. At stage 3, the T2 domain becomes a circle, thus creating a new posterior tenascin domain (T3). The depressor muscle becomes anchored on T2 and grows anteriorly. At stage 4, the depressor muscle establishes connections between T2 of one bud and T3 of the anterior neighboring bud. Tenascin domain 4 (T4) emerges at the bottom of the circle enclosed by T2 and T3. At stage 5, the anterior end of the erector muscle emerges and is attached to T4. At stage 6, the erector muscle is connected between T4 of a bud and T1 of its posterior neighboring bud and then criss-crosses the depressor muscle. At stage 7, the muscles become mature. (*B* and *C*) Schematic drawings from the top and side views of the transformation from stage 1–7. (*D*) Schematic drawing showing the three levels of depth in the dermis, based on confocal images (n = 5). (Scale bars: *A*, 100 μm.)

integrin family of heterodimers, including integrin β1 (13). We carried out immunostaining for integrin β1 expression during muscle pattern formation (E9 and E10). Integrin β1 appears to be expressed on two cell types: on cells in the base of feather buds and on muscle fibers. To observe the intensity dynamics of integrin β1 clearly, we separated the bottom of the feather bud into three parts (T2, T3, and T4) based on the designation in Fig. 2. We found that the expression level of integrin β1 seems to be more stable on the cells in the base of feather buds and to be more dynamic on the muscle fibers (Fig. 3 *K–M*). At E9, integrin β1 is expressed at low levels in the muscle cells in the T2 domain (muscle cells expressing integrin strongly will become yellow). At E10, many muscle cells become yellow in the T2 domain, indicating that stabilized muscle fibers coexpress integrin β1 strongly. However, there was no significant difference in the expression intensity of integrin β1 in the nonmuscle region of T4 between E9 and E10 (Fig. 3 *K–M*). These results suggest that tension, produced by the connection of muscle fibers between two feather buds, can increase integrin β1 expression as judged by immune reactivity. However, whether the mechanism is direct or indirect remains to be studied.

To study the function of integrin β1 in the anchoring process, we added the neutralizing integrin β1 antibody (V2E9; Developmental Studies Hybridoma Bank) to the culture media of E8 skin for 2 d. In treated skin, tenascin C levels were elevated in the anterior bud mesenchyme compared with those of the controls. The depressor muscle connections were weak, and most muscle cells were located at feather bud boundaries. However, in the control group, the connection was robust, which resembled the physiological muscle connection at E10 (Fig. 3 *N* and *N′*). After quantitative analysis, we found that muscle width, length, and relative compactness were significantly higher in the control group than in the integrin β1 neutralized group. However, the distances between buds were higher in the integrin β1 neutralized group than in the control group (Fig. 3*O*). These data suggest that tenascin C may play a role in attachment and anchoring for muscle cells via integrin β1.

We summarize the findings from Figs. 2 and 3 here as follows: (*i*) The tenascin C domains mark the starting point for outwardly migrating muscle fibers; (*ii*) the muscle fibers initially migrate radially in the interbud dermis, and after a number of fibers connect to a bud, stabilization of connected muscle fibers ensues, leading to the formation of consolidated depressor muscle bundles; and (*iii*) after the depressor muscle connection forms, the erector muscle connections are established following the same rules. Spatial restrictions and temporal control in each follicle during the assembly process ensure correct layering of the network.

The Intradermal Smooth Muscle Network Is Adaptive. We then asked whether the muscle network can adjust its configuration in response to changing environmental stimuli. To induce a change in the environment, we injured the muscle network by ablating a single feather bud in an E8 skin explant (dorsal-pelvic tract region). After 2 d in culture, feather depressor muscle fibers from neighboring buds began to reroute toward their new nearest neighbor buds, as evidenced by the unusually long muscle bundles between nearest

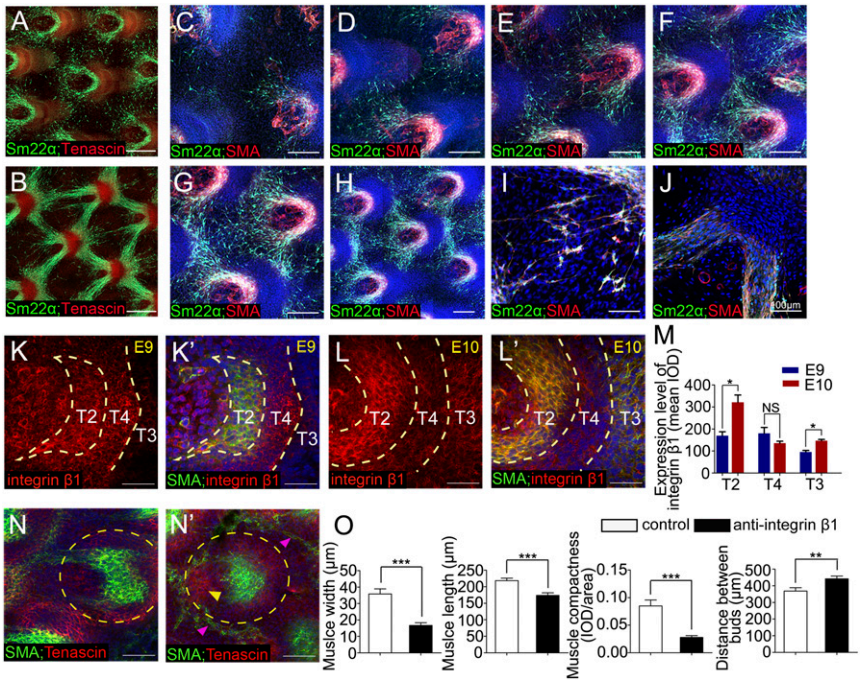

Fig. 3. Formation of muscle anchoring sites on feather follicles and conversion from scattering smooth muscle cells to stabilized muscle bundles. (*A* and *B*) Formative process. Smooth muscle cells (SM22α immunostaining, green) emit from each feather bud and navigate centrifugally, covering a wide range of angles at E9, before becoming stabilized muscle bundles connecting feather nodes (tenascin C immunostaining, red) at E10 ($n = 3$). (*C–H*) Developmental series from E9 to E10 showing the muscle progenitors cover the great majority of interbud space before stabilized muscle bundles are formed. The muscle cells are stained with SM22α (green), SMA (red), and DAPI (blue). Areas devoid of feather muscle cells correspond to tenascin-positive regions ($n = 3$). (*I* and *J*) At E10, muscle bundles have formed and feather muscle cells change their morphology, growing longer and having blobs protruding from their cell bodies ($n = 3$). (*K*, *K′*, *L*, and *L′*) Bottom of the feather bud at stages E9 and E10 was stained with integrin β1 (red), SMA (green), and DAPI (blue). The T2, T3, and T4 regions separated by broken lines were based on the designation in Fig. 2. Integrin β1 and SMA show positive coexpression (yellow) in muscle cells in *K′* and *L′* ($n = 3$). (*M*) Expression level of integrin β1 in T2, T3, and T4 regions was compared between E9 and E10 ($n = 3$). IOD, integrated optical density; NS, not significant. (*N* and *N′*) Neutralization of integrin β1 binding with integrin β1 antibody in E8 skin explant for 2 d results in the appearance of altered tenascin domains (yellow arrowhead) in the dermis. The loosely connected muscle fibers detached from the tenascin domains and located in the interbud space (purple arrowheads) ($n = 3$). (*O*) Muscle width, length, relative compactness, and distances between buds were compared between anti-integrin β1 and control groups ($n = 3$). An unpaired *t* test was applied in *M* and *O* (*$P < 0.05$; **$P < 0.01$; ***$P < 0.001$). Data presented are mean ± SEM. (Scale bars: *A–H*, 200 μm; *I*, *K*, and *L′*, 50 μm; *J*, *N*, and *N′*, 100 μm.)

neighboring buds (Fig. 4 *A* and *A′*). Thus, the muscle network can adapt to the loss of a node and establish new connections to adjacent buds.

The orientation of feather buds is plastic and can respond to epithelial signals to reorient before Hamburger and Hamilton stage 33 (E7.5), as shown through epithelium/mesenchyme recombination studies (14). Branched buds or a disordered bud pattern can form when the recombination process is carried out on more mature buds (15). To investigate this observation further, we performed a recombination study on E7 dorsal skin. The epithelium was separated from the dermis and then recombined after the epithelium was rotated 90°. After 3 d in culture, the orientation of the developing feathers and feather depressor muscles turned 90°, following the orientation of the epithelium (Fig. 4 *B* and *B′*). Thus, the muscle network topology is plastic and is dependent on feather orientation. To investigate whether the network configuration is based on the epithelium or the dermis, we recombined the femoral epithelium onto the dorsal mesenchyme. After 3 d in culture, the depressor muscle pattern resembles that of the dorsal tract (Fig. 4 *C* and *C′*). Thus, the muscle network topology is dependent on the relative positions of feather buds in the dermis.

The above experiments demonstrate that muscle patterning adapts to the local environment. We also wonder whether the body-wide muscle network adapts to the mechanics of the whole embryo. Because elongation is most significant along the A-P axis during development, we excised a band of the dorsal skin perpendicular to the A-P axis in ovo at E8 to break the continuity of the dorsal skin and observed the changes of the muscle network (Fig. 4*D*). After incubation for 2 d, the embryo grew to a normal size, although the wound was still present (Fig. 4*E*). We found that in the midline of the skin, A-P feather muscle connections weakened and muscle fibers were inclined to grow laterally. The angle between the two "arms" of the depressor muscles became enlarged (Fig. 4*E′*). In contrast, A-P connections were very robust under physiological conditions at E10 (Fig. 4*E″*). These data suggest that the muscle network can be regulated globally by breaking the continuity of the skin along the A-P axis. The relaxation of A-P tension may account for this phenomenon. As a whole, this result demonstrates that the macroscale muscle pattern within the skin can respond as a whole, adapting to new tension conditions, following wounding in ovo.

Next, we explored whether a muscle network could also be reassembled in the reconstituted skin assay. In the feather reconstitution assay, dissociated mesenchymal cells confronted with a piece of same-sized epithelium could self-organize into a periodic pattern without previous cues or sequential propagation (8). For this experiment, epithelium and mesenchyme were separated from E7.5 skin. The dermis was then completely dissociated to individual cells by digestion with 2% trypsin for 15–20 min at 4 °C. The

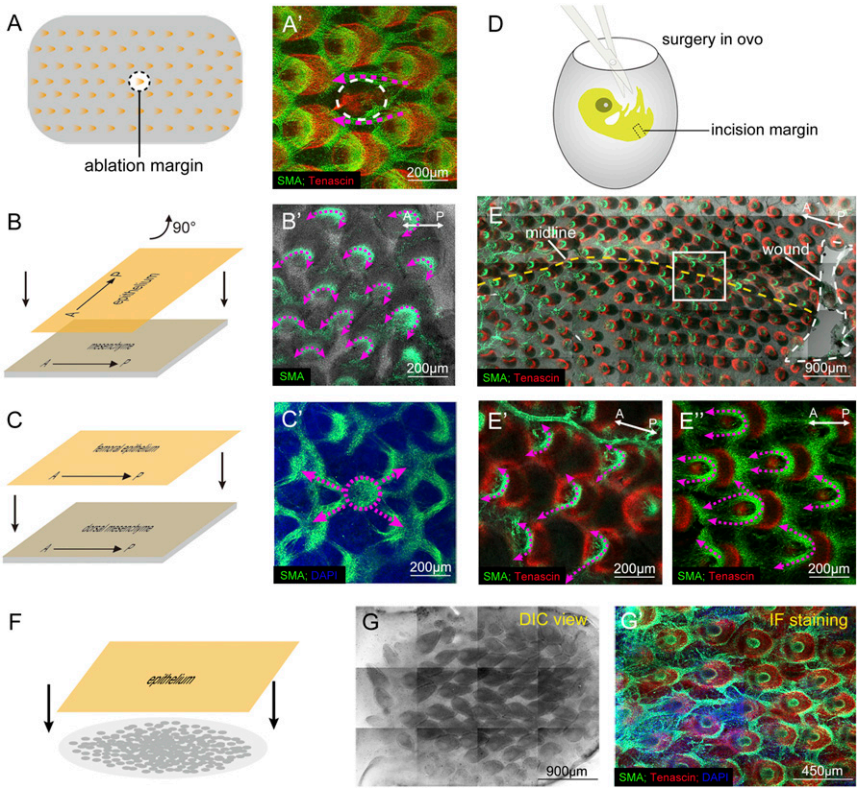

Fig. 4. Muscle network is adaptive and regenerative. To test the robustness of the muscle network, we challenged the formed network with wounding and recombination, and we also reconstituted feather patterns after cell dissociation. Immunofluorescence of SMA (green) and tenascin C (red) is used to follow changes in the network configuration. (*A* and *A′*) Adaptation of muscle patterns after ablation of a feather bud. The white dotted line in *A′* shows the position of the ablated bud. The purple dotted lines indicate that the muscle fibers reorient to their new nearest neighbor ($n = 3$). (*B*, *B′*, *C*, and *C′*) Adaptation of muscle patterns after epithelial/mesenchymal recombination. (*B* and *B′*) E8 skin was recombined after the dorsal epithelium was turned 90° relative to the dermis along its A-P axis. After 3 d in culture, the muscle orientation turned correspondingly ($n = 3$). (*C* and *C′*) E8 dorsal tract dermis was recombined with the femoral epithelium. After 3 d in culture, the muscle pattern resembled that of the dorsal tract ($n = 3$). (*D*, *E*, and *E′*) Adaptation of muscle patterns after a skin incision perpendicular to the A-P axis ($n = 3$). (*D*) Band of skin was cut off in the midline of the dorsal-pelvic tract in ovo at E8. After 2 d of incubation, the embryo grew to a normal size, although the wound had not healed. (*E*, *E′*, and *E″*) Harvested skin shows thinner A-P muscle connections (purple arrows) compared with E10 control skin (*E″*). The boxed area in *E* is magnified in *E′*. (*F*, *G*, and *G′*) Adaptation of muscle patterns in reconstituted skin. (*F*) Skin is reconstituted using dissociated dermal cells and intact epidermis. (*G* and *G′*) After 3 d in culture, dermal cells are able to reform muscle connections once the feather array reforms ($n = 3$). DIC, differential interference contrast; IF, immunofluorescence.

dissociated dermal cells were plated and then overlaid with intact epithelium (Fig. 4*F*). In this process, positional identity (originally in the bud or interbud) is lost and the cells assume newly induced identities. Surprisingly, after reconstitution, depressor muscle fibers were able to develop and generate a network between the feather buds (Fig. 4 *G* and *G′*). Thus, when cell position identity is lost, feather buds are formed first and muscle networks can then self-organize to reform patterns with the feather buds as reference points.

Mechanical Force Modulates the Muscle Network Patterns. We next sought to identify the local rules that guide feather muscle connections. We noticed that the A-P depressor muscle connections in the dorsal-pelvic tract diminished after in vivo ablation of a skin band (Fig. 4 *D* and *E′*). As such, we hypothesized that weakened A-P tension through the whole dorsal skin may account for the muscle pattern transformation. To test this, we first cultured skin explants on a restrained collagen gel (Fig. 5*A*). The feather muscle network pattern was able to develop similar to that seen in vivo. Tenascin C, known to respond to mechanical tension, formed a thin, clearly demarcated ring (Fig. 5*B*).

We then designed a simple apparatus that allowed us to apply tension on the collagen gel and skin explant. The collagen gel was poured over two strips of Velcro, which were then pinned to Sylgard. After culturing for 2 h, when the skin explant became attached to the gel, the pin was plucked and the skin explant, together with the gel and Velcro, was floating in the media. In addition, external tension was applied to lengthen the collagen gel along the longitudinal or vertical axis by positioning the pins (Fig. 5*A*). Thus, we cultured skin explants on collagen gels at natural, floating, or extended lengths to understand the effect of external tension.

When skin explants were cultured on floating collagen gels for 2 d, the skin contracted significantly. The Velcro strips on the two ends helped to prevent normal collagen gel contraction. Under these conditions, the expression of SMA was diminished, except in the periphery of the skin explant. Tenascin C did not show the sharply demarcated ring shape seen in the skin explant cultured on a restrained gel (Fig. 5*C*). We also performed this experiment and harvested the floating skin explant early at day 1. The skin size was similar to that of the control, and the dramatic contraction did not happen. SMA was expressed weakly in the midline of the skin explant, maybe due to the weak residual tension between the skin explant and the floating gel. In most regions of the skin, there was no SMA expression. Tenascin C did not show the sharply demarcated ring shape either (*SI Appendix*, Fig. S5). As a result, we conclude that the expression of SMA is tension-sensitive and that the muscle fibers do not form in the absence of tension.

Next, we tried to gauge the response of developing feather muscles to externally applied tension. When tension was applied along the A-P axis (longitudinal) or vertical axis (lateral), the skin deformed significantly (Fig. 5 *D* and *F*). The tension was sustained for 2 d in culture until the skin was harvested. In the longitudinal tension group, most depressor muscle bundles grew

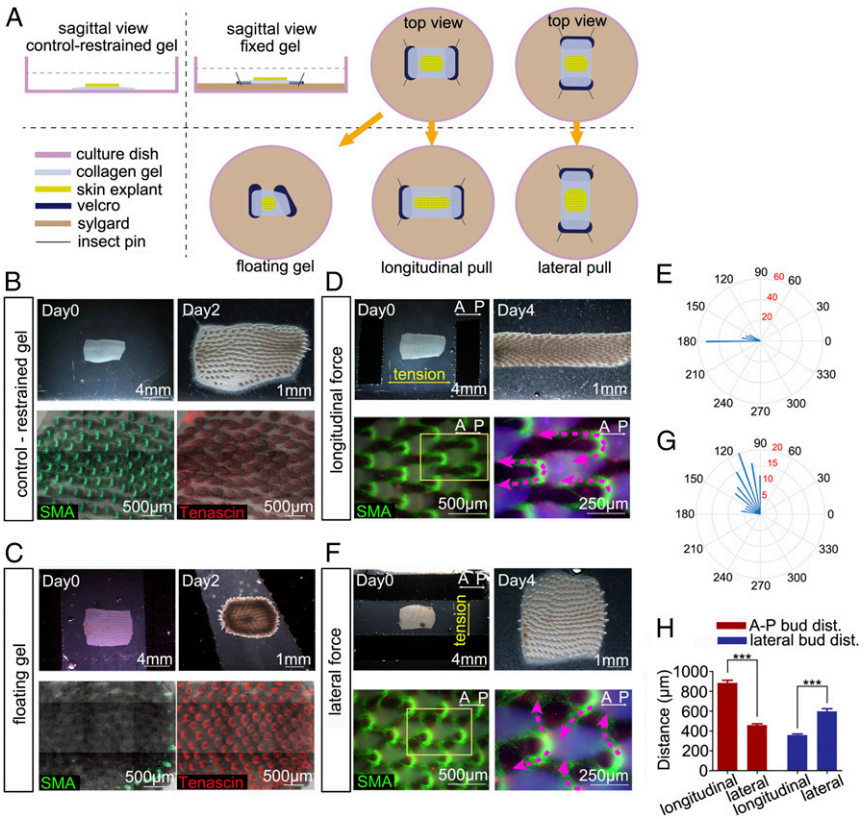

Fig. 5. Mechanical force modulates the network pattern. (*A*) Schematic drawings showing skin explants on restrained and fixed collagen gels, the mechanical force apparatus, the floating gel, and the longitudinal and lateral pull experiments. (*B–D* and *F*) Immunofluorescence of SMA (green) and tenascin C (red) of the cultured skin ($n = 3$). (*B*) E8 skin cultured on the restrained gel for 2 d showed a muscle and tenascin pattern similar to that found in vivo. (*C*) E8 skin cultured on floating gel for 2 d showed contracted skin with diminished muscle patterning, except at the tissue periphery. (*D* and *E*) E8 skin subjected to externally applied tension along the A-P axis (longitudinal) (*D*, *Upper Right*) resulted in muscle bundles that grew along the A-P axis (broken lines). (*F* and *G*) E8 skin subjected to tension perpendicular to the A-P axis (lateral) (*F*, *Upper Right*) resulted in muscle bundles that grew laterally (broken lines). (*E* and *G*) Angles of muscle bundles were calculated and analyzed ($n = 100$). (*H*) Bud distance (dist.) along the A-P axis and D-V axis between longitudinal and lateral force groups was compared ($n = 8$; unpaired t test, $^{***}P < 0.001$). Data presented are mean ± SEM.

anteriorly along the A-P axis and the angles between two arms were close to 180° (Fig. 5 *D* and *E*). In the lateral tension group, most depressor muscle bundles grew more laterally and the angles were close to 90° (Fig. 5 *F* and *G*). To exclude the interference factor of bud distance in muscle patterning, we compared the interbud distances along the A-P and dorsal-ventral (D-V) axes between longitudinal and lateral force groups. We found that the interbud distance along the A-P axis in the longitudinal force group was significantly larger than that in the lateral force group, and the interbud distance along the D-V axis in the longitudinal force group was significantly smaller than that in the lateral force group (Fig. 5*H*). The results showed the muscle connections align with the tension regardless of the enlarged distance between buds. These data strongly suggest that mechanical force is a significant guiding factor involved in muscle fiber migration.

As we observed a tendency of developing skin to contract in the floating gel experiment, we then wondered whether the muscle network pattern would be affected when this intrinsic contraction force is inhibited. First, we inhibited the rho-associated protein kinase (ROCK) with Y27632. ROCK is known to be involved in regulating cell migration by promoting cellular contraction (16). With Y27632, the skin became more relaxed and muscle fibers became more radially symmetrical. Feather muscles could not find correct destinations and no longer formed stable muscle connections with neighboring buds (Fig. 6 *A*–*B*″). Second, we tried to inhibit the contraction of developing skin using the myosin IIb inhibitor, blebbistatin; most muscle fibers failed to establish stable connections (Fig. 6 *C*–*C*″). In contrast, the muscle bundles became stable and robust in control explant cultures, similar to the physiological pattern (Fig. 6 *A*– *A*″).

We quantified the differences between these three groups. We found that (*i*) the muscle length of the Y27632-treated group was shorter than that of the control group; (*ii*) the muscle width of the Y27632-treated group was much wider than that of the control group, probably due to the relaxation of the muscle bundles; and (*iii*) the compactness of drug-treated groups became much lower than that of the control group (Fig. 6*D*).

We also analyzed the interbud distance in explants treated with inhibitors. We observed that the interbed distance of the Y27632-treated group became larger than that of the control group (Fig. 6*D*). Together, these results suggest that the balance between the intrinsic and externally applied tensions plays an important role in the morphogenesis of feather muscles.

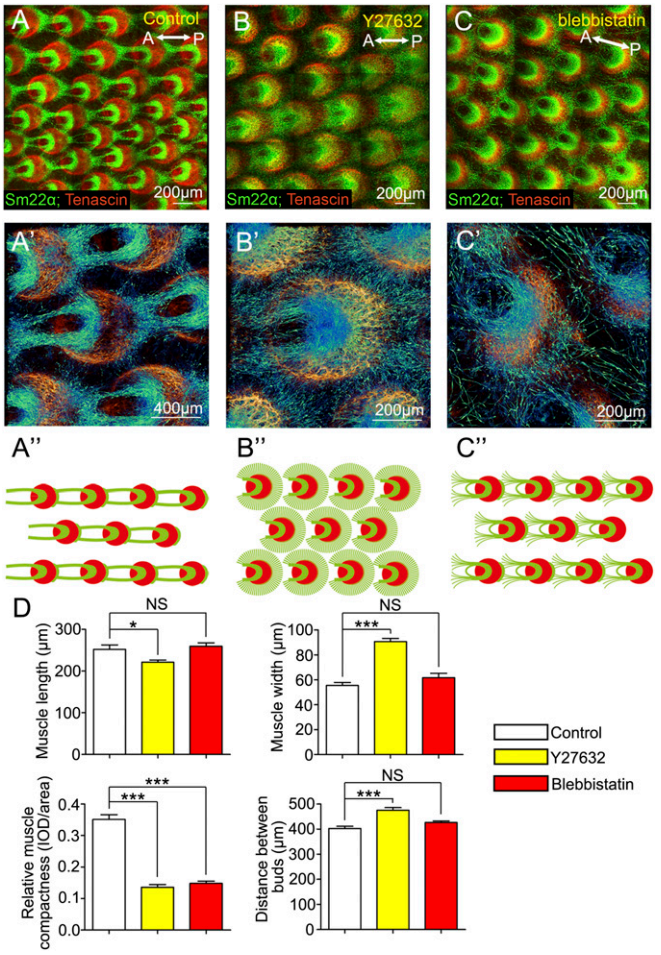

Fig. 6. Balance between intrinsic and outward tension of the skin affects network patterning. (*A*–*C*) Immunofluorescence of Sm22α (green) and tenascin (red) of E8 skin cultured for 2 d on collagen gels. (*A*′, *B*′, and *C*′) Three-dimensional reconstructions of local regions from *A*–*C*. (*A*″, *B*″, and *C*″) Schematic drawings from the top views of the groups in *A*–*C*. (*A*, *A*′, and *A*″) Control group cultured on the restrained gel for 2 d had a similar muscle and tenascin pattern to that observed in vivo ($n = 3$). (*B*, *B*′, and *B*″) In E8 skin cultured on the restrained gels for 2 d with Y27632 (10 μM), feather muscles no longer formed muscle connections with neighboring buds ($n = 3$). (*C*, *C*′, and *C*″) In E8 skin cultured on restrained gels for 2 d with blebbistatin (10 μM), most muscle fibers did not form stable connections ($n = 3$). (*D*) Muscle length, width, relative compactness, and distances between buds were compared between control, Y27632, and blebbistatin groups ($n = 11$). One-way ANOVA and Bonferroni's multiple comparison test were used to compare all of the pairs (*$P < 0.05$; ***$P < 0.001$). IOD, integrated optical density; NS, not significant.

Computational Modeling Demonstrates the Mechanisms Required for Efficient and Adaptive Patterning. To test our hypotheses regarding the efficient development, and adaptive nature, of the feather muscle network, we developed a simplified computational model of muscle fiber migration/elongation and attachment (Fig. 7 and *SI Appendix*, Fig. S6 and Table S1). The patterning process initiates within the feather buds, from which muscle fibers emerge.

We simulate growth of the muscle fiber network using an on-lattice random walk model. Muscle fibers are initiated at the center of each node and follow a biased random walk that guides the muscle fibers to make the initial contacts. We assume that at each update step, a fiber "tip" can move up, down, left, or right on the square lattice, and that the fiber extends along the path taken by the tip. If, during its random walk, the fiber tip touches a new node, the tip connects to this node. Fibers can disconnect at random, and the fiber tip then begins its random walk again. The random walks of the fiber tips are assumed to be biased to form connections to neighboring buds by two mechanisms. The first is an endogenous guidance cue (that may be biochemical or biomechanical) that is preexisting in the tissue. This cue effectively ensures that, in the absence of any other fibers, the fiber tips undergo a biased random walk toward neighboring nodes and will be connected when they meet the neighboring buds. The second guidance cue is provided by earlier fibers that are connected between two nodes: Later fiber tips are biased to move toward target nodes that are connected to the node from which the fiber extends. Without these cues, the time taken for fiber tips to find another node is prohibitive, and very few fibers are connected at any one time.

The bias of each muscle fiber's individual random walk evolves as the network of attached fibers extends, representing the reinforced biochemical and/or biomechanical guidance cues within the microenvironment. Thus, muscle fibers that make initial contacts between neighboring nodes help guide later growing muscle fibers toward the existing muscle bundle in a positive feedback loop. To incorporate network plasticity, we propose that a certain percentage of connected fibers can detach and begin the random walk process again, until reattachment occurs. Further details of the algorithm are given in *Materials and Methods*.

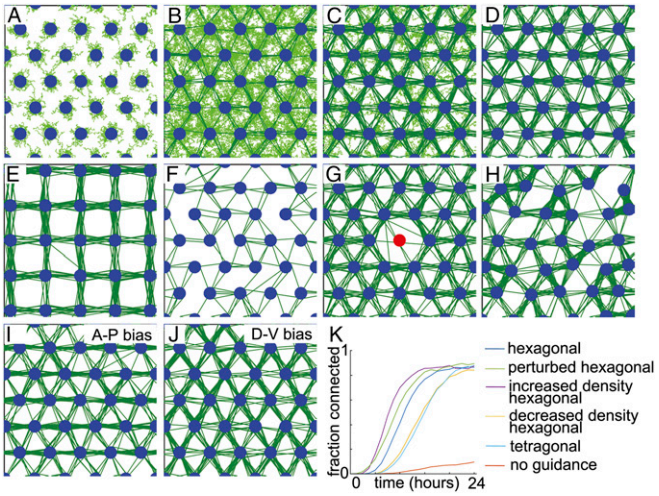

Fig. 7. Computational model validates the mechanisms required for efficient and adaptive patterning. (*A–J*) Growth of the muscle fiber network was simulated with an on-lattice random walk model. Feather buds are marked in blue, unconnected muscle fibers in light green, and connected muscle fibers in dark green. (*A–C*) Growth of the feather muscle network as individual fibers elongate through the tissue. As connections between nearest-neighbor buds establish, a self-generated guidance field emerges that stabilizes the network. Stabilized networks with different bud configurations are shown: hexagonal (*D*) and tetragonal (*E*). (*F*) In the absence of guidance cues, the network is sparse, with few connected fibers at any time. (*G*) Ablation of a feather node (red dot) leads to reattachment of the muscle fibers to nearby feather nodes. (*H*) Perturbation of bud positions leads to a distorted network, with most fiber connections still between nearest-neighbor feather buds. (*I* and *J*) Feather muscle networks generated under a global tension bias. (*I*) With an A-P bias, the number of connections in the A-P direction (left to right in the figure) increases. (*J*) With a D-V (lateral) bias, the number of connections in the D-V direction (up to down in the figure) increases. (*K*) Temporal evolution of the network in terms of the fraction of connected fibers: hexagonal, dark blue; perturbed, green; increased density hexagonal, purple; decreased density, yellow; square, light blue; no guidance, orange.

In our lattice-based random walk model, the muscle fibers extend from the centers of the feather buds and elongate by a biased random walk until they eventually connect with another bud (Fig. 7 *A–D* and *SI Appendix*, Fig. S6). As a result of this random migration process, the muscle fibers initially infiltrate most of the interbud space and eventually form connections between feather buds. Upon connection with the tenascin C domains of other buds, the fibers consolidate to occupy the shortest path connection between the buds they connect (Fig. 7*D*).

In a hexagonal array, as in the dorsal-pelvic tract, the fibers connect to their nearest-neighbor buds (Fig. 7*D*). With a different packing topology of buds, the patterns change. For example, in the femoral tract, the pattern is maintained in a tetragonal configuration (Fig. 7*E*). In the absence of any guidance cues, network formation is sparse, with few connected fibers at any time (Fig. 7*F*).

Our modeling efforts demonstrate that guidance cues are necessary to establish the networks observed experimentally: Fiber tips must be biased to move toward neighboring buds by biochemical or biomechanical cues, with the strength of the bias increasing as the number of connections between the originating node and the target node increases (Fig. 7 *A–D*). This latter hypothesis is supported by the fact that the expression level of integrin β1 was increased after muscle connections and tension were established (Fig. 3 *K* and *L*).

Our model predictions are consistent with the range of experimental observations made under perturbations: (*i*) Ablation of a feather node leads to reattachment of the muscle fibers to nearby feather nodes (Fig. 7*G*); (*ii*) with perturbation of bud positions from the usual hexagonal arrangement, leading to a distorted network, most fiber connections are still between nearest-neighbor feather buds (Fig. 7*H*); and (*iii*) with global tissue tension biased along either the A-P axis or D-V axis, the fibers thicken along the A-P axis or D-V axis, respectively (Fig. 7 *I* and *J*).

To better understand the model results, we compared temporal evolution of the plastic networks under different conditions, in terms of the fraction of connected fibers. With guidance provided by biochemical and/or biomechanical cues, the fraction of connected fibers increases over time and the fraction of connected fibers increases as bud density increases. However, without any guidance cues, the fraction of connected fibers is low at any time because the rate of attachment is close to the rate at which fibers detach (Fig. 7*K*).

Discussion

Connecting the Dots: How Intradermal Smooth Muscle Fibers Establish Their Origin and Insertion Sites on Feather Follicles. Feathers are arranged to form a feather coat that endows the body with an aerodynamically streamlined physique. Feather muscles can adjust feather orientation to cover each body region with a smooth surface, and also adjust the angle of attack of flight feathers to enhance aerodynamics. The pleomorphic topology of feather muscle network patterns across different skin tracts reflects a flexible method for network adaptation to regional variations in feather density.

The formation of intradermal muscle networks in birds utilizes an economical design in which the muscle fibers initially migrate out of the feather buds in all directions, but then consolidate upon contacts with neighboring buds. The interbud region is too vast for the muscle fibers to accurately and efficiently find their distant anchoring points without external guiding cues. We found the chicken embryo has solved this problem by sending radiating muscle fibers out of each feather bud over a broad angle range, and then stabilizing and concentrating the whole bundle along the direction of an established muscle connection. This interpretation is supported by the finding that scattering muscle fibers are located at the anchoring points (Figs. 1*D*, 2, and 3 *C–E*). During this formative process, the first connected fiber plays the leading role for the rest of the muscle fibers. This mechanism resembles the nerve growth cone with radiating filopodia that probe their local environments. The growth cone responds by turning toward the source of attractive guidance cues, which is one mechanism regulating axon targeting (17, 18). In this case, it is a chemical cue. In the muscle case here, it is a mechanical cue.

Tenascin-C is expressed abundantly in normal myotendinous junctions and is a traditional tendon marker (19). In developing feather follicles, it progressively exhibits four topological domains for muscle initiation. In mouse hairs, during the myogenesis of arrector pili muscles, tenascin-C is confined to the bulge in telogen follicles but displays a more widespread distribution in the anagen phase of the hair cycle (9). Tenascin functions as the ligand of integrin α8β1 and mediates cell adhesion (13). In feathers, we found that integrin β1 plays an essential role in mediating muscle–tenascin interactions. This finding is supported by the suppression of muscle connection using antibodies to integrin β1.

The Avian Intradermal Muscle Network Is Dynamic and Adaptive. Here "adaptive" patterning is used in two aspects. The first is during network assembly; smooth muscle fibers use existing feather buds as the cue to build a network pattern. Second, once the feather muscle network is formed, the network still can adapt to physiological and environmental changes. The muscle network ensures avians can move their feathers synergistically to maximize temperature maintenance, courtship displays, and aerodynamics under changing flight conditions (5). Instead of forming a network, in mammalian hair, arrector pili are attached to one single follicle. Although the orientation of individual hair follicles is

determined by global and local sources of polarity, the orientation of the arrector pili closely adapts to that of the associated follicle (20, 21).

Recent work suggests mechanical forces also play a central role in cell fate determination, tissue morphogenesis, and directional cell motility (22–24). These intrinsic mechanical forces are generated in the contractile actin cytoskeleton of living cells. The mechanical interactions between cells and the extracellular matrix (ECM) play a central role in controlling cell fate, shape, proliferation, and tissue patterning. Regarding the formation of feather buds themselves, it has recently been shown that the contractility-driven cellular pulling contributes to the feather bud pattern formation (25). In the next tissue morphogenesis stage, the work here shows mechanical force can play a patterning role again, using the existing buds as reference points. We found that the outgrowing muscle fibers were guided by the tension lines between buds. On a macroscopic level, the anisotropic tension distribution, caused by the differential growth over the body, leads to the muscle network configuration.

While muscle/myoblast differentiation has been the focus of numerous studies, the mechanism that establishes muscle patterning is much less well understood. Considering the fact that the muscle connections between two buds contain both depressor and erector muscles, a core issue of this patterning process is how the criss-crossed muscle fibers can avoid connecting to inappropriate sites (i.e., erector muscles binding to depressor sites and vice versa). One model put forth, based upon *Drosophila* abdominal wall muscle patterning, is that the muscle cells of different groups follow distinct chemical gradients within their environment (26–28). Another model, established both in limb and craniofacial muscles, is that both the migration and patterning of myoblasts are determined by the prepattern of connective tissues (29–32). Both the canonical Wnt pathway transcription factor Tcf4 and the T-box transcription factors Tbx4/5 are expressed in the muscle connective tissue, which is critical for the patterning of limb muscles (30, 31). Similarly, the connective tissues, which are derived from cranial neural crest cells, regulate the migration and patterning of muscle precursors in the craniofacial region (29, 32). We postulate that, in a similar fashion, feather muscle fibers might use collagen and other ECM constituents as guides to reach their nearest neighbors. The molecular mechanism of this mechanosensing is a major direction of future investigation.

Here, in the feather muscle model, we demonstrate that both mechanical forces and tension distributions provide clues for connection patterns. Four distinct tenascin domains, which emerge sequentially, form a bowl-like structure whose upper (or lower) edge provides the starting or insertion points for muscle fibers. The insertion sites of depressor or erector muscles appear just after establishment of the corresponding tenascin domains. Thus, muscle fiber connections are dictated by the spatiotemporal distribution of the tenascin domains. In A-P connections, the depressor muscles are established first, followed by the erector muscles, following similar processes to establish another layer of the muscle network later in time.

A Bioinspired Algorithm for Network Self-Assembly. Based on the experimental findings here, we summarize the formative process of the intradermal muscle network in the chicken as follows: (*i*) Each bud produces several tenascin C- and integrin-expressing domains as anchoring points; (*ii*) muscle fibers emit from each feather bud, initially extending uniformly radially; (*iii*) when multiple muscle fibers reach the tenascin C domains of nearby feather buds, they form stable connections and other fibers either join the stable bundle or disappear; and (*iv*) the process repeats itself to set up depressor and elevator muscle fibers in two waves of assembly. Spatial restriction and temporal order ensure the correct assembly of this network.

Surprisingly, the network pattern formed here is not rigid, but is adaptable. After its formation, the balance between intrinsic contraction and externally applied forces can still modulate muscle patterning. Mechanical forces and the resulting tension distributions provide guidance cues for muscle fibers to reorient. Upon injury or loss of feather follicles, muscle fibers that lost their connected follicles can be reconnected to new follicle partners following similar mechanical cues.

Our qualitative model provides a useful framework to frame and test our hypotheses. Under our model, in the absence of guidance cues, muscle fibers can still form connections with their nearest neighbors via unbiased random walks, but these connections take an incredibly long time to form. Facilitated by mechanical or chemical cues, stabilized bundles can form more effectively. Allowing a small fraction of fibers to detach and reattach after the network is formed confers robustness of the network; the network becomes adaptive, able to respond to changing applied mechanical force to realign muscle fibers along new tension lines.

Our work was inspired by the complex organization of the avian integumentary musculature system (5, 10). We set out to understand how this complex architecture is built. We found that the intradermal dermal muscle network weaves feather follicles into one large functional unit, enabling new collective behavior at the integument level (5, 33). Through an adaptive patterning process, the smooth muscle network can respond to alterations of mechanical forces in a changing environment.

Materials and Methods

Experimental Model. Fertilized pathogen-free eggs were purchased from Charles River Laboratories. Chicken embryos were staged according to the method described by Hamburger and Hamilton (34).

Skin Explant. E7–8 dorsal skins between the lower neck and the tail were dissected and placed on the membrane of a tissue culture insert in a six-well plate. Explants were grown in 2 mL of DMEM with 2% FBS in a humidified 5% CO_2 incubator at 37 °C for the indicated time period. Y27632 (10 μM, Y0503; Sigma) or blebbistatin (10 μM, 1852; Tocris Bioscience) was added into certain groups. The procedures of recombination and reconstitution are provided in *SI Appendix, Materials and Methods*.

Surgery in Ovo. The fertilized egg was incubated at 38 °C until E8. The operation was performed under the dissecting microscope. The top of the eggshell was broken carefully with the tip of forceps. The chorioallantoic membrane was broken, and the amnion cavity was then exposed. The amniotic membrane was broken carefully, and the position of the embryo was adjusted. A band of skin perpendicular to the A-P axis in the midline of the dorsal-pelvic tract was cut off with microscissors. The broken eggshell was covered by a plastic membrane to maintain the humidity inside the egg. The egg was put back into the incubator. The sample was harvested 2 d later.

Establishment of Mechanical Force Apparatus. In the restrained-gel experiments, rat tail tendon collagen I (354236; BD Biosciences) was dissolved in 1× PBS and its pH was adjusted to 7.0 with 1 N NaOH before being added to the culture dish. In the external tension experiments, dishes were coated with Sylgard 184 (Dow Corning) before the Velcro (Velcro BVBA) and collagen gel were set on the surface. The Velcro was cut into small bands, treated with 70% EtOH for 20 min, rinsed in HBSS twice, and left to air-dry. The Velcro bands were then embedded in the gel. Insect pins were used to fix the Velcro bands onto Sylgard 184. Skin explants were placed on the top of collagen gel and cultured. To create the force, the insect pins were pulled out, moved toward a certain direction, and fixed at the new position.

Whole-Mount Immunostaining. Skin samples were dissected, followed by dehydration in a mixture of methanol and dimethyl sulfoxide (DMSO) (vol/vol = 4:1) at 4 °C overnight. The samples were bleached in a mixture of methanol, DMSO, and 30% H_2O_2 (vol/vol/vol = 4:1:1) for 20 min, and then washed with Tris-buffered saline Tween-20 (TBST) for 10 min twice. After being incubated in blocking buffer for 2 h, the samples were incubated with a 1:50–200 dilution of antibody at 4 °C overnight. After being washed four times in TBST for 1 h, the samples were incubated with a 1:500 dilution of

secondary antibodies at 4 °C overnight (details are provided in *SI Appendix, Materials and Methods*).

In Situ Hybridization. RT-PCR was performed using E7 chicken embryo mRNA. Degenerate primers used for chicken MyoD are as follows: forward, ccgccgatgacttctatgac; reverse, gtgctccagcactgggtagt. The correct-sized bands were extracted from agarose gels and cloned into pDrive Cloning Vector (231224; Qiagen). Chicken Pax3 plasmid was kindly donated by Martyn D. Goulding's laboratory, The Salk Institute for Biological Studies, La Jolla, CA (35). The probe was made by the reaction of the mixture of linearized plasmid DNA, digoxigenin-labeling mix (11277073910; Roche), transcription buffer, and T7 RNA polymerase (10881767001; Roche). The staining procedure and more details are provided in *SI Appendix, Materials and Methods*.

Three-Dimensional Reconstruction. Whole-mount fluorescence of the embryo skin was performed, and the serial images were aligned using ImageJ software (version 1.36b; NIH). The tenascin domains and muscles surrounding the bud were reconstructed using Amira software (Visage Imaging).

Computational Model Algorithm. The model algorithm is provided as follows:

i) Initialize the feather node pattern: (*a*) Generate a square lattice (lattice spacing step_length); (*b*) set the node positions, and specify the bud diameter (d); (*c*) initialize the fibers to extend from each node (fibers_per_node): for each fiber, place a random walker (fiber tip) at its node; and (*d*) set time = 0.

ii) While time < time_final, update the network. At each step: (*a*) For each connected fiber tip, disconnect the fiber tip with probability adapt_prob, and if the fiber tip disconnects, place the fiber tip at its position adapt_undo time steps previously; (*b*) for each disconnected fiber tip: calculate the left-to-right bias of the random walk (rho_x) and the up-to-down bias of the random walk (rho_y); update the position (up, down, left, or right a distance step_length) using the probabilities of the tip moving up [prob_up = (1 + rho_y)/4], down [prob_down = (1 − rho_y)/4], left [prob_left = (1 − rho_x)/4], or right [prob_right = (1 + rho_x)/4]; and if the fiber tip moves within distance d/2 of a node, connect the tip to this node; and (*c*) let time = time + 1.

rho_x = epsilon * cos(angle_of_nearest_node) * (guidance_parameter * bud_diameter/(2 * distance_to_nearest_node) + feedback_parameter * (1 + number_connections_ between_originating_and_nearest_node)/(1 + fibers_per_node)

rho_y = epsilon * sin(angle_of_nearest_node) * (guidance_parameter * bud_diameter/(2 * distance_to_nearest_node) + feedback_parameter * (1 + number_connections_ between_originating_and_nearest_node)/(1 + fibers_per_node)

The algorithm of the model under perturbations is provided in *SI Appendix, Materials and Methods*.

Quantification and Statistical Analysis. One-way ANOVA and unpaired *t* test analyses were applied with GraphPad Prism. One-way ANOVA analysis was applied for the comparisons between three groups. Bonferroni's multiple comparison test was used to compare all of the pairs (Fig. 6*D* and *SI Appendix*, Fig. S2 *A* and *B*). An unpaired *t* test was applied for the comparisons between two groups (Figs. 3 *M* and *O* and 5*H* and *SI Appendix*, Figs. S2*C* and S4*E*). Significance of statistical tests is reported in figure graphs as follows: ***$P < 0.001$; **$P < 0.01$; *$P < 0.05$.

The angles of muscle bundles were calculated and analyzed with MATLAB 7 (MathWorks). The sample size was 100 bundles for each group (Fig. 5 *E* and *G*).

ACKNOWLEDGMENTS. We thank the Imaging Core of the University of Southern California Research Center for Liver Diseases for support. We thank Dr. Christopher Chen and Dr. Li Ming Fu for comments on the manuscript. This work was funded by National Institute of Arthritis and Musculoskeletal and Skin Diseases Grants R01 AR060306 and AR047364; National Institute for General Medical Sciences Grant GM 125322; and National Natural Science Foundation of China Grant 81400478. R.E.B. is a Royal Society Wolfson Research Merit Award Holder and a Leverhulme Research Fellow.

1. Benson AR, Gleich DF, Leskovec J (2016) Higher-order organization of complex networks. *Science* 353:163–166.
2. Hütt MT, Kaiser M, Hilgetag CC (2014) Perspective: Network-guided pattern formation of neural dynamics. *Philos Trans R Soc Lond B Biol Sci* 369:20130522.
3. Sporns O (2014) Contributions and challenges for network models in cognitive neuroscience. *Nat Neurosci* 17:652–660.
4. Tero A, et al. (2010) Rules for biologically inspired adaptive network design. *Science* 327:439–442.
5. Homberger DG, de Silva KN (2003) The role of mechanical forces on the patterning of the avian feather-bearing skin: A biomechanical analysis of the integumentary musculature in birds. *J Exp Zoolog B Mol Dev Evol* 298:123–139.
6. Chuong CM, Yeh CY, Jiang TX, Widelitz R (2013) Module-based complexity formation: Periodic patterning in feathers and hairs. *Wiley Interdiscip Rev Dev Biol* 2:97–112.
7. Lai YC, Chuong CM (2016) The "tao" of integuments. *Science* 354:1533–1534.
8. Jiang TX, Jung HS, Widelitz RB, Chuong CM (1999) Self-organization of periodic patterns by dissociated feather mesenchymal cells and the regulation of size, number and spacing of primordia. *Development* 126:4997–5009.
9. Fujiwara H, et al. (2011) The basement membrane of hair follicle stem cells is a muscle cell niche. *Cell* 144:577–589.
10. Lucas AM, Stettenheim PR (1972) *Avian Anatomy: Integument* (Agricultural Research Services, US Department of Agriculture, Washington, DC), 1st Ed, Vol 2.
11. Olivera-Martinez I, Coltey M, Dhouailly D, Pourquié O (2000) Mediolateral somitic origin of ribs and dermis determined by quail-chick chimeras. *Development* 127:4611–4617.
12. Scaal M, Christ B (2004) Formation and differentiation of the avian dermomyotome. *Anat Embryol (Berl)* 208:411–424.
13. Schnapp LM, et al. (1995) The human integrin alpha 8 beta 1 functions as a receptor for tenascin, fibronectin, and vitronectin. *J Biol Chem* 270:23196–23202.
14. Chuong CM, Widelitz RB, Ting-Berreth S, Jiang TX (1996) Early events during avian skin appendage regeneration: Dependence on epithelial-mesenchymal interaction and order of molecular reappearance. *J Invest Dermatol* 107:639–646.
15. Chen CW, Jung HS, Jiang TX, Chuong CM (1997) Asymmetric expression of Notch/Delta/Serrate is associated with the anterior-posterior axis of feather buds. *Dev Biol* 188:181–187.
16. Sit ST, Manser E (2011) Rho GTPases and their role in organizing the actin cytoskeleton. *J Cell Sci* 124:679–683.
17. Dent EW, Gertler FB (2003) Cytoskeletal dynamics and transport in growth cone motility and axon guidance. *Neuron* 40:209–227.
18. Kalil K, Li L, Hutchins BI (2011) Signaling mechanisms in cortical axon growth, guidance, and branching. *Front Neuroanat* 5:62.
19. Järvinen TA, et al. (2003) Mechanical loading regulates the expression of tenascin-C in the myotendinous junction and tendon but does not induce de novo synthesis in the skeletal muscle. *J Cell Sci* 116:857–866.
20. Chang H, Nathans J (2013) Responses of hair follicle-associated structures to loss of planar cell polarity signaling. *Proc Natl Acad Sci USA* 110:E908–E917.
21. Cetera M, Leybova L, Woo FW, Deans M, Devenport D (2017) Planar cell polarity-dependent and independent functions in the emergence of tissue-scale hair follicle patterns. *Dev Biol* 428:188–203.
22. Engler AJ, Sen S, Sweeney HL, Discher DE (2006) Matrix elasticity directs stem cell lineage specification. *Cell* 126:677–689.
23. Petridou NI, Spiró Z, Heisenberg CP (2017) Multiscale force sensing in development. *Nat Cell Biol* 19:581–588.
24. Chien YH, Srinivasan S, Keller R, Kintner C (2018) Mechanical strain determines cilia length, motility, and planar position in the left-right organizer. *Dev Cell* 45:316–330.e4.
25. Shyer AE, et al. (2017) Emergent cellular self-organization and mechanosensation initiate follicle pattern in the avian skin. *Science* 357:811–815.
26. Baylies MK, Bate M, Ruiz Gomez M (1998) Myogenesis: A view from Drosophila. *Cell* 93:921–927.
27. Schnorrer F, Kalchhauser I, Dickson BJ (2007) The transmembrane protein Kon-tiki couples to Dgrip to mediate myotube targeting in Drosophila. *Dev Cell* 12:751–766.
28. Schweitzer R, Zelzer E, Volk T (2010) Connecting muscles to tendons: Tendons and musculoskeletal development in flies and vertebrates. *Development* 137:2807–2817.
29. Borue X, Noden DM (2004) Normal and aberrant craniofacial myogenesis by grafted trunk somitic and segmental plate mesoderm. *Development* 131:3967–3980.
30. Hasson P, et al. (2010) Tbx4 and tbx5 acting in connective tissue are required for limb muscle and tendon patterning. *Dev Cell* 18:148–156.
31. Kardon G, Harfe BD, Tabin CJ (2003) A Tcf4-positive mesodermal population provides a prepattern for vertebrate limb muscle patterning. *Dev Cell* 5:937–944.
32. Rinon A, et al. (2007) Cranial neural crest cells regulate head muscle patterning and differentiation during vertebrate embryogenesis. *Development* 134:3065–3075.
33. Widelitz R, Chuong CM (2016) Quorum sensing and other collective regenerative behavior in organ populations. *Curr Opin Genet Dev* 40:138–143.
34. Hamburger V, Hamilton HL (1951) A series of normal stages in the development of the chick embryo. *J Morphol* 88:49–92.
35. Bang AG, Papalopulu N, Kintner C, Goulding MD (1997) Expression of Pax-3 is initiated in the early neural plate by posteriorizing signals produced by the organizer and by posterior non-axial mesoderm. *Development* 124:2075–2085.